Available online at www.sciencedirect.com
SCIENCE DIRECT®
Journal of Power Sources 124 (2003) 1–11
JOURNAL OF POWER SOURCES
www.elsevier.com/locate/jpowsour

A mathematical model for PEMFC in different flow modes

Shan-Hai Ge, Bao-Lian Yi*

Fuel Cell R&D Center, Dalian Institute of Chemical Physics, Chinese Academy of Sciences, Dalian 116023, China

Abstract

A two-dimensional, steady state model for proton exchange membrane fuel cell (PEMFC) is presented. The model is used to describe the effect of flow mode (coflow and counterflow), operation conditions and membrane thickness on the water transport, ohmic resistance and water distribution in the membrane, current density distribution along the channel and performance of PEMFC. Effect of liquid water on the transport in the two-phase region of cathode diffusion layer was considered. Water transport in the membrane by electro-osmosis drag, diffusion and convection were combined in this model. The model predicts that the dry reactant gases can be well internally humidified and maintain high performance when PEMFC is operated in the counterflow mode without external humidification. Counterflow mode does not show any advantageous while the reactant gases are high humidified or saturated. Compared to the coflow mode, counterflow mode improves the current density distribution with dry or low humidity gases. The higher the anode is humidified, the more water will migrate from anode to cathode. The modeling results compare very well with experimental results.

Keywords: Proton exchange membrane fuel cell; Water transport; Mathematical model; Flow mode; Counterflow

1. Introduction

Proton exchange membrane fuel cells (PEMFCs) are efficient and environmentally clean electrical generators that are being developed for both stationary and mobile applications [1–4]. Over the past decade, significant research effort of PEMFC has been focused on fuel cell structure design, the development of better catalyst, the better structure of catalyst layer and gas diffusion layer, the development of membrane with high performance, thermal and water management [5].

In the PEMFC application, high membrane conductivity is one of the key parameters for attaining high performance. The most commonly used exchange membrane in fuel cell is Nafion (DuPont). The proton conductivity of Nafion membrane increases with the water content [6,7]. In order to maintain high water content of membrane along the channel, the reactant gases are humidified by passing them through humidifiers. High humidity of reactant gases may lead to liquid water existed in the cathode. When cathode is flooded, the diffusion of reactant gas through its pores is difficult. For the H_2/O_2 system, water flooding is known to be the main limiting factor that restricts the improvement of performance at high current densities [8]. In addition, external humidification of the reactant gases is a burden for the fuel cell system. In order to simplify the subsystem and reduce heat removal from the PEMFC stacks, operation of PEMFCs without external humidification of the reactant gases is advantageous for the PEMFC system [9]. Qi designed a double-path-type flow-field that has two gas inlets and two gas outlets for PEMFCs. Such a design enables the entering dry reactant gases to be dydrated by the exiting gas [10]. The problem of water transport in PEMFC with different humidification conditions has been the object of several experimental and theoretical studies [6,11–15].

Models for water management are useful for describing and getting great insight into the mass transport processes. One-dimensional PEMFC models were developed in the early 1990s by Bernardi and Verbrugge [14] and Springer et al. [13]. In the hydraulic model developed by Bernardi and Verbrugge [14], the author assumes that the membrane is fully saturated with water and that most of the water is transported through the electrodes in the liquid phase. This model may be not applicable in the case of feeding dry or unsaturated reactant gases. Springer et al. [13] presented a diffusion model. Water transport in the membrane by means of electro-osmotic drag and back diffusion process at different humidification conditions was described in detail in the diffusion model. Springer et al. [6] assumed that the presence of liquid water only modifies the effective porosity for oxygen gas transport whereas Bernardi assumed that a constant liquid volume fraction and no interactions between

* Corresponding author. Tel.: +86-411-4379097; fax: +86-411-4684839.
E-mail address: blyi@dicp.ac.cn (B.-L. Yi).

0378-7753/$ – see front matter © 2003 Elsevier B.V. All rights reserved.
doi:10.1016/S0378-7753(03)00584-6

Nomenclature

a	electrode length (m)
b	electrode width (m)
c	concentration of water in the membrane (mol/m^3)
c_f	fixed charge concentration in membrane (mol/m^3)
D	diffusion coefficient (m^2/s)
D_m	diffusion coefficient of water in the membrane (m^2/s)
E_0	open circuit potential (V)
E_{cell}	cell potential (V)
f	local fraction of the water produced that evaporates through the anode
F	Faraday constant (96,485 C/mol)
I	local current density (A/m^2)
I_0	exchange current density (A/m^2)
k_p	hydraulic permeability of water in membrane (m^2/s)
m	molecular weight (g/mol)
M	mole flow (mol/s)
n_d	electro-osmotic drag coefficient
N	mole flux (mol/(m^2 s))
p	pressure (Pa)
p_{BM}	logarithmic average value of nitrogen partial pressure (Pa)
R	universal gas constant (8.314 J/(mol K))
R_{co}	contact resistance (Ω m^2)
R_m	membrane resistance (Ω m^2)
s	liquid water saturation
T	temperature (K)
x	direction along the channel length (m)
x_i	mole fraction of species i
y	direction across the cell (m)

Greek letters

α	water relative humidity
δ	thickness (m)
δ_{ij}	Angstrom unit
Ω_D	dimensionless function of the temperature and of the intermolecular potential field for the molecules of i and j
ε	porosity
η	electrode overpotential (V)
λ	water content of membrane
μ	water viscosity (Pa s)
σ	membrane conductivity (Ω m)$^{-1}$
ξ	stoichiometric flow ratio of reaction gas

Superscripts and subscripts

0	initial value
a	anode
av	average
c	cathode
d	diffusion
e	electro-osmotic drag
H	hydrogen
ij	species i, j
m	membrane
O	oxygen
p	pressure
w	water

liquid and gas flow. One-dimensional model is so simple that it neglects the variations of water content of membrane and gas concentration along the flow channel. It cannot be used to optimize operation conditions and to predict performance of PEMFC with high working surface area.

To investigate and optimize the distribution of gas component, water content of membrane, current density and net water transport along the flow channel, two-dimensional models were developed in recent years [15–23]. Fuller and Newman [15] simulated a PEMFC operation under the condition of moist gas in electrodes. In this model, concentrated solution theory is used for description of the membrane. The water distribution in the membrane and the net water flux across it were obtained. Nguyen and White [16] compared three humidification designs using a combined heat and mass transfer model. Both Fuller and Nguyen consider coflow pattern to study transfer processes.

Recently, Gurau et al. [17] presented a comprehensive model for the entire sandwich of a PEMFC including the gas channels. Similarly, Hsing and Futerko [18] developed a two-dimensional model of coupled fluid flow, mass transport and electrochemistry of PEMFC operating without external humidification of hydrogen and air streams. Hsing assumed a constant local current density in the model. Dannenberg et al. [19] presented an along-the-channel mass and heat transfer model for a PEMFC and an agglomerate approach was used for the description of the active layer of the cathode. Yi and Nguyen [20] analyzed multicomponent transport in porous electrodes of PEMFCs using the interdigitated gas distributors. It should be noted that all these models do not account for the mass transport processes in the present of liquid water.

During PEMFC operation, especially at low stoichiometric flow rate of reactant gases, liquid water is likely to appear in the cathode, resulting in two-phase transport phenomena. Wang et al. [21] modeled the two-phase flow and transport in the air cathode of PEMFCs and concluded that capillary action was the dominant mechanism for water transport inside the two-phase zone of the hydrophilic structure. The transport processes become significantly complicated in the two-phase zone. A two-dimensional, two-phase, multicomponent, transient model was developed by Natarajan for the cathode of the PEMFC [22]. It was found that the performance of the cathode was dominated by the dynamics of

liquid water, especially in the high current density range. Neglecting the transport of dissolved reactant gases, this liquid phase in the electrode is a one-component system. Janssen [23] reported that the presence of a gradient in the chemical potential of liquid water could produce a flux.

The aim of the present work was to develop a model that describes, in steady state, the water transport in the membrane and the fuel cell performance, at dry and different humidified gases in the coflow and counterflow modes. Effect of liquid water on the effective porosity for gas transport in the cathode was considered in this model. Such a study will be useful for the design and operation of practical PEMFC stacks.

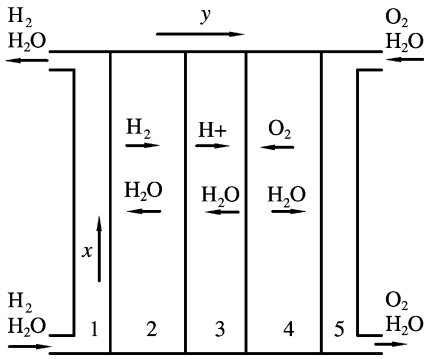

Fig. 1. A schematic of PEMFC regions: (1) anode flow channel; (2) gas diffusion anode; (3) membrane; (4) gas diffusion cathode; (5) cathode flow channel.

2. Experimental and model development

Membrane electrode assemblies (MEA) of 140 cm^2 were prepared using Nafion 112 and Nafion 117 membranes (DuPont) and electrodes made by our groups containing 0.4 mg/cm^2 platinum (20% Pt/Vulcan XC-72 carbon powder, Cabot Corp.) The membrane was first pretreated using a usual procedure, i.e. maintained in 3% H_2O_2 at 353 K for 1 h, then washed with pure water. The membrane was then maintained in 0.5 mol/l H_2SO_4 at 353 K for 1 h and washed with pure water. Electrodes were impregnated with recast Nafion solution (Aldrich) by brushing. The MEA was prepared by hot-pressing a membrane sheet between the two electrodes.

Pure hydrogen and oxygen were used as reactant gases, and stoichiometry of hydrogen and oxygen were kept at needed values. The electrical parameters of the cell were controlled by an automatically test station interfaced to a personal computer. The amount of water exiting the cell at the anode and cathode gas outlets was measured by condensing the water in an ice trap and then by weighting the condensed water. For water transport measurements, the cell was operated in the constant-current mode.

2.1. Model assumptions

A two-dimensional, steady state, water transport model for a PEMFC is developed. A schematic illustration of a PEMFC in the counterflow mode is shown in Fig. 1. The model regions consist of a membrane sandwiched between two gas diffusion electrodes, the anode flow channel and cathode flow channel. The model accounts for the water content of membrane, the mass transport of water and other gaseous species across the cell (*y*-direction), and current density distribution along the flow channel (*x*-direction, direction of the hydrogen flow). To keep the water transport model simple, a few assumptions are made.

1. The temperature is assumed to be uniform throughout the membrane electrode assembly and gas channels.
2. An ideal gas mixture is assumed. In the flow channel, a plug-flow condition is assumed, and pressure drop along the channel is neglected. The gases and liquid water are treated as being perfectly well mixed in the *y*-direction.
3. The diffusion layer is uniform and the mass transport in the electrodes is considered only along the *y*-direction.
4. It is assumed that the catalyst layer is ultra-thin, gas diffusion through the catalyst layer is assumed to be negligible.
5. Water contents of membrane on the interface of both sides are assumed to be in equilibrium with water vapor in gases. The mass transport of hydrogen and oxygen in the membrane is negligible. Water transport in the membrane is considered only along the *y*-direction.
6. It is assumed that liquid water transport is not a limited process. How liquid water is transferred in the cathode is not included in this model. It is assumed that the change in gas pressure caused by capillary effects is small enough to have a negligible effect on gas transport.
7. Electrode pores for gas flow are separated from pores for liquid water. Liquid water modifies the effective porosity for oxygen gas transport in the cathode diffusion layer and affects the cathode overpotential.

2.2. Mass balance

There are three water transport mechanisms in the membrane [24]: (i) electro-osmotic drag, which is caused by proton transport from the anode side to the cathode side of the membrane; (ii) back-diffusion by the concentration gradient of water, the concentration gradient is due to the transport of water by the electro-osmotic drag and the production of water at the cathode via the oxygen reduction reaction; and (iii) convection generated by pressure gradient within the pores of the proton exchange membrane.

In a calculated unit of membrane, there is no potential gradient in the *x*-direction. The electro-osmotic drag flux in *y*-direction, $N_{w,y,e}$, is as follows

$$N_{w,y,e} = n_d \frac{I(x)}{F} \quad (1)$$

where n_d is the electro-osmotic drag coefficient (number of water molecules carried by a proton), $I(x)$ the local current density of the fuel cell, and F the Faraday's constant. There is no pressure gradient within the membrane in the x-direction, so convection generated by pressure gradient is

$$N_{w,y,p} = -\frac{k_p}{\mu} c \frac{dp}{dy} \tag{2}$$

where k_p, μ, p and c are the hydraulic permeability of water in membrane, water viscosity, pressure and concentration of water in the membrane, respectively. Diffusion flux is as follows

$$N_{w,y,d} = -D_m \frac{\partial c}{\partial y} \tag{3}$$

$$N_{w,x,d} = -D_m \frac{\partial c}{\partial x} \tag{4}$$

where D_m is the diffusion coefficient of water. As the thickness of membrane is much less than its length (y is less than x by several orders), the diffusion of water in the membrane in x-direction can be neglected. The calculated results will show that concentration gradient of water in y-direction is higher several orders than that in x-direction. n_d and D_m were measured by Springer et al. [13]

$$n_d = \frac{2.5\lambda}{22} \tag{5}$$

$$D_m = 10^{-10} \exp\left[2416\left(\frac{1}{303}\right) - \left(\frac{1}{T}\right)\right] \times (2.563 - 0.33\lambda + 0.0264\lambda^2 - 0.000671\lambda^3), \quad \lambda > 4 \tag{6a}$$

Eq. (6a) is the fit for $\lambda > 4$, as for $2 > \lambda < 4$, D_m can be expressed as

$$D_m = 10^{-10} \exp\left[2416\left(\frac{1}{303}\right) - \left(\frac{1}{T}\right)\right] \times (-1.25\lambda + 6.65), \quad 3 > \lambda < 4 \tag{6b}$$

$$D_m = 10^{-10} \exp\left[2416\left(\frac{1}{303}\right) - \left(\frac{1}{T}\right)\right] \times (2.05\lambda - 3.25), \quad 2 > \lambda < 3 \tag{6c}$$

where λ is the water content of membrane (water molecule per SO_4^-). According to Bernardi and Verbrugge [25], the pressure profile through the membrane region is linear, and the velocity is constant.

$$\frac{dp}{dy} = \frac{p_c - p_a}{\delta_m} \tag{7}$$

Water concentration is calculated as follows

$$c = \lambda c_f \tag{8}$$

where c_f is the fixed charge concentration in membrane. The water flux through the membrane (y-direction) can be written as follows

$$N_{w,y} = \frac{2.5\lambda}{22}\frac{I(x)}{F} - \frac{k_p}{\mu}\lambda c_f \frac{p_c - p_a}{\delta_m} - D_m c_f \frac{d\lambda}{dy} \tag{9}$$

In the anode, gas diffusion in x-direction is much less than that in y-direction, and therefore gas diffusion in x-direction is neglected. Stefan–Maxwell equation is used to describe anode mass transport.

$$\frac{dx_i}{dy} = \sum_{j=1}^{n} \frac{RT}{pD_{ij}^{eff}}(x_i N_j - x_j N_i), \quad i = 1, 2, \ldots, k \tag{10}$$

where D_{ij}^{eff} is an effective binary diffusivity of the pair i–j, T the temperature, and R the universal gas constant. We relate the effective diffusion coefficient to the diffusion coefficient in a nonporous system D_{ij} by [25]

$$D_{ij}^{eff} = D_{ij}\varepsilon^{1.5} \tag{11}$$

Binary diffusion coefficients D_{ij} can be calculated by using the equation commended by Bird et al. [26]

$$D_{ij} = 1.8583 \times 10^{-7} \frac{\sqrt{T^3[(1/m_i) + (1/m_j)]}}{(p/p_0)\delta_{ij}^2 \Omega_D} \tag{12}$$

where m_i, m_j are the molecular masses of i and j, respectively, δ_{ij} the Angstrom unit, Ω_D the dimensionless function of the temperature and of the intermolecular potential field for the molecules of i and j.

At steady state, the fluxes of all the diffusing species in the pores are constant, and the amount of water produced by the electrochemical reaction is equal to the amount of water transported through the pores of diffusion layer. The flux of hydrogen, oxygen and water can be described [27].

$$\frac{I(x)}{2F} = -2N_O = N_H = -N_w^a + N_w^c \tag{13}$$

The parameter f is defined as the local fraction of the water produced that evaporates through the anode layer.

$$f = \frac{-N_w^a}{-N_w^a + N_w^c} = 1 - \frac{N_w^c}{-N_w^a + N_w^c} \tag{14}$$

$$f_{av} = \frac{1}{aI_{av}} \int_0^a fI\,dx \tag{15}$$

where a is the length of channel, I_{av} the average current density. For two components (H_2O, H_2), Eq. (10) can be solved. The concentration distribution of water in the anode diffusion layer, $x_w^a(y)$, and anode hydrogen flux are obtained

$$x_w^a(y) = \frac{f + (1-f)x_w^a}{1-f} \times \left[\frac{f + (1-f)x_w^{m,a}}{f + (1-f)x_w^a}\right]^{y/\delta_a} - \frac{f}{1-f}, \quad f \neq 1 \tag{16}$$

$$N_{\mathrm{H}} = \frac{p_{\mathrm{a}} D^{\mathrm{eff}}_{\mathrm{H\text{-}w}}}{RT\delta_{\mathrm{a}}} \frac{1}{1-f} \ln\left[\frac{f+(1-f)x^{\mathrm{m,a}}_{\mathrm{w}}}{f+(1-f)x^{\mathrm{a}}_{\mathrm{w}}}\right], \quad f \neq 1 \tag{17}$$

Eqs. (16) and (17) are not fit for $f = 1$. As for $f = 1$, $x^{\mathrm{a}}_{\mathrm{w}}(y)$ and N_{H} are

$$x^{\mathrm{a}}_{\mathrm{w}}(y) = \frac{y}{\delta_{\mathrm{a}}}(x^{\mathrm{m,a}}_{\mathrm{w}} - x^{\mathrm{a}}_{\mathrm{w}}) + x^{\mathrm{a}}_{\mathrm{w}}, \quad f = 1 \tag{18}$$

$$N_{\mathrm{H}} = \frac{p_{\mathrm{a}} D^{\mathrm{eff}}_{\mathrm{H\text{-}w}}}{RT\delta_{\mathrm{a}}}(x^{\mathrm{m,a}}_{\mathrm{w}} - x^{\mathrm{a}}_{\mathrm{w}}), \quad f = 1 \tag{19}$$

At the inlet region of cathode, humidified or dry oxygen enters the fuel cell, and no liquid water exits in the flow channel and electrode. Stefan–Maxwell equation, Eq. (8), is used to describe cathode mass transport in this single-phase region.

While oxygen flow along the flow channel, oxygen is humidified by water produced by electrochemical reaction. Liquid water exits in the cathode as oxygen is saturated and effect of liquid water on the transport in the two-phase region of cathode diffusion layer is considered. Electrode pores for gas flow are assumed to separate from pores for liquid water. In the pore of diffusion layer for gas flow, steam pressure is saturated and concentration gradient of inert impurity gases, e.g. nitrogen, is formed. It is obvious that the nitrogen flux is zero in steady state. The oxygen flux though the cathode diffusion layer in two-phase region is described as follows:

$$N_{\mathrm{O}} = \frac{D^{\mathrm{eff}}_{\mathrm{O\text{-}w}} p_{\mathrm{c}}}{RT\delta_{\mathrm{c}} p_{\mathrm{BM}}}(p_{\mathrm{O}} - p^{\mathrm{m}}_{\mathrm{O}}) \quad \text{and} \quad p_{\mathrm{BM}} = \frac{p_{\mathrm{B2}} - p_{\mathrm{B1}}}{\ln(p_{\mathrm{B2}}/p_{\mathrm{B1}})} \tag{20}$$

p_{BM} is the logarithmic average value of nitrogen partial pressure on both side of cathode diffusion layer. Liquid water modifies the effective porosity for oxygen gas transport in the cathode diffusion layer [22].

$$D^{\mathrm{eff}}_{\mathrm{O\text{-}w}} = D_{\mathrm{O\text{-}w}}[\varepsilon(1-s)]^{1.5} \tag{21}$$

where s is the liquid water saturation. The presence of liquid water in the porous gas diffusion layer results in mass transport limitations imposed by the restriction of gas diffusion pores [22].

While reactant gases flow along the flow channel (gas chamber of fuel cell), hydrogen or oxygen transport from channel to diffusion layer and water transport from diffusion layer to channel. In the coflow mode, it can be obtained that

$$M_{\mathrm{H}}(x) = \xi_{\mathrm{a}} b \int_0^a N_{\mathrm{H}}\,\mathrm{d}x - b\int_0^x N_{\mathrm{H}}\,\mathrm{d}x \tag{22}$$

$$M_{\mathrm{O}}(x) = \xi_{\mathrm{c}} b \int_0^a N_{\mathrm{O}}\,\mathrm{d}x - b\int_0^x N_{\mathrm{O}}\,\mathrm{d}x, \quad \text{(coflow)} \tag{23}$$

$$M^{\mathrm{a}}_{\mathrm{w}}(x) = M^{\mathrm{a}}_{\mathrm{w},0} + b\int_0^x f N_{\mathrm{H}}\,\mathrm{d}x \tag{24}$$

$$M^{\mathrm{c}}_{\mathrm{w}}(x) = M^{\mathrm{c}}_{\mathrm{w},0} + b\int_0^x (1-f) N_{\mathrm{H}}\,\mathrm{d}x, \quad \text{(coflow)} \tag{25}$$

where ξ is the stoichiometric flow ratio of reaction gas, the ratio of the amount of reactant gases added to the fuel cell to the amount that is required by the electrochemical reaction; b is width of electrode. On the counterflow operation, oxygen and water mole flow rates are

$$M_{\mathrm{O}}(x) = (\xi_{\mathrm{c}} - 1) b \int_0^a N_{\mathrm{O}}\,\mathrm{d}x + b\int_0^x N_{\mathrm{O}}\,\mathrm{d}x, \quad \text{(counterflow)} \tag{26}$$

$$M^{\mathrm{c}}_{\mathrm{w}}(x) = M^{\mathrm{c}}_{\mathrm{w},0} + b\int_0^a (1-f) N_{\mathrm{H}}\,\mathrm{d}x - b\int_0^x (1-f) N_{\mathrm{H}}\,\mathrm{d}x, \quad \text{(counterflow)} \tag{27}$$

A fit of the relationship of λ versus water relative humidity (water vapor activity), α, used in the model is [13]

$$\lambda = 0.043 + 17.81\alpha - 39.85\alpha^2 + 36.0\alpha^3, \quad a < 1 \tag{28a}$$

$$\lambda = 14.0 + 1.4(\alpha - 1), \quad 1 \le a \le 3 \tag{28b}$$

$$\lambda = 16.8, \quad a \ge 3 \tag{28c}$$

$$\alpha = x_{\mathrm{w}} \frac{p}{p^{\mathrm{sat}}} \tag{29}$$

2.3. Cell potential and current density

The cell voltage (E_{cell}) is calculated from the resistance (include membrane resistance and contact resistance, R_{co}), current density and electrode overpotentials, as follows:

$$E_{\mathrm{cell}} = E_0 - \eta(x) - (R_{\mathrm{m}} + R_{\mathrm{co}}) I(x) \tag{30}$$

In the most of model, the contact electrical losses at the interfaces between different fuel cell elements are neglected [6,15–17]. Contact resistance is taken into account in this model.

A fit of the relationship of membrane conductivity versus λ is [13]

$$\sigma_T = \exp\left[1268\left(\frac{1}{303} - \frac{1}{T}\right)\right] \times (0.5139\lambda - 0.326), \quad \text{for } \lambda > 1 \tag{31}$$

While λ is less than 1, the membrane conductivity was assumed constant. The membrane resistance is

$$R_{\mathrm{m}} = \int_0^{\delta_{\mathrm{m}}} \frac{1}{\sigma_T}\,\mathrm{d}y \tag{32}$$

Anode overpotential, when pure hydrogen is used, is small and is neglected in the calculation. Electrode overpotential in the model only includes cathode overpotential. $\eta(x)$ can be calculated from the following equation [21].

$$\eta(x) = \frac{RT}{0.5F} \ln\left[\frac{I}{I_0(p^{\mathrm{c}}_{\mathrm{O}}/p_0)(1-s)}\right] \tag{33}$$

here I_0 is the exchange current density. The model exchange current density parameter was adjusted to yield results

that suitably mimic the experimental results. Liquid water formed at the interface can cover the active reaction sites. It is assumed that the active reaction sites decrease linearly with increase in the liquid water saturation. To account for this coverage phenomenon the $(1 - s)$ term is include in Eq. (33). The average current density for a given cell voltage is calculated by integrating along the whole channel length.

$$I_{av} = \frac{1}{a}\int_0^a I(x)\,dx \tag{34}$$

2.4. Solution technique

The inlets of hydrogen and oxygen are in the same site in coflow mode. The model equations are solved numerically at a given value of average current density, I_{av}. Based on I_{av}, mole flow rate of hydrogen, oxygen and water are calculated in the inlet of gas channel. The E_{cell} and a values of $I(x)$ are initially guessed, and one-dimensional equations for the mass transport in electrodes and membrane are solved. Then f and distribution of water content are obtained. The local current density is calculated and compared with the specified value. If the calculated value disagrees with the specified one, a new value of $I(x)$ is given. This process is repeated until the calculated $I(x)$ agrees with the specified one. This procedure is then repeated at $x = dx$, and until in the whole flow channel. Therefore, I_{av} is calculated using Eq. (34) and compared with the initial given value. A value of E_{cell} is given again and secant method is used to help search for the correct E_{cell} value.

The solution process with counterflow mode is similar to that with coflow mode. The site of the inlet of hydrogen is the outlet of oxygen. A mole flow rate of water in the cathode at $x = 0$ is assumed. The mole flow rate of water in cathode at $x = a$ is calculated and compared with the actual value. The mole flow rate of water in cathode at $x = 0$ is obtained using secant method.

3. Results and discussion

Correct water management has been found to be important to maintain high proton conductivity of membrane and achieve high performance for PEMFCs. A mathematical model of PEMFC is very useful and effective tool to optimize cell designs and operation conditions. In this section, this model will be used to evaluate flow modes and various operation conditions (relative humidity, temperature and pressure differential) and to investigate the effect of membrane thickness on the performance of a PEMFC. Table 1 lists the important parameters of electrode and membrane used as the base case.

3.1. Comparison of the calculated and experimental results

Fig. 2 compares the calculated fuel cell potential as a function of current density with experimental data. Electrode area of 140 cm^2 and Nafion 112 membrane are used in this test. The fuel cell is operated with dry gases in the counterflow mode. It can be found that modeling results compare very well with the experimental results.

Table 1
Parameter values of electrode and membrane used as the base case

Parameter	Value
E_{cell}	1.05 V
I_0	40 A/m^2
c_f	1.2×10^3 mol/m^3*
k_p	1.8×10^{-18} m^2*
μ	3.56×10^{-6} Pa S*
δ_m	
Nafion 117	1.75×10^{-4} m
Nafion 115	1.25×10^{-4} m
Nafion 1135	0.80×10^{-4} m
Nafion 112	0.50×10^{-4} m
a	0.12 m
δ_a	3.0×10^{-4} m
ε_a	0.4
δ_c	3.0×10^{-4} m
ε_c	0.4
R_{co}	1×10^{-5} Ω m^2

* [14].

We have measured the fraction of product water leaving the anode side of a PEMFC over a wide range of operation conditions. Table 2 shows the comparison of the calculated and experimental values for f_{av} at different operation conditions. Nafion 117 membrane is used in this test. The fuel cell is operated in coflow mode. The temperature of fuel cell is kept constant at 353 K. It can be found that calculated values for f_{av} agreed with the experimental results. Tests 1–3 show that water transfer from anode to cathode increases with increasing relative humidity of feeding hydrogen.

3.2. Effect of relative humidity of reactant gases

In the following sections, the effect of various cell operating parameters and membrane thickness are investigated

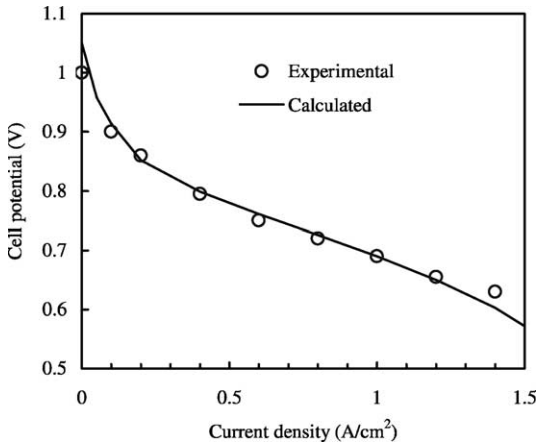

Fig. 2. Comparison between the model predictions and experimental results when Nafion 112 membrane is used ($T = 353$ K, $p_a = p_c = 3 \times 10^5$ Pa, $\xi_a = 1.25$, $\xi_c = 2.0$, $\alpha_a = \alpha_c = 0$).

Table 2
Calculated and experimental values for f_{av}

Test	ξ_a	ξ_c	α_a	α_c	p_a ($\times 10^5$ Pa)	p_c ($\times 10^5$ Pa)	I_{av} (A/cm^2)	$f_{av,exp}$	$f_{av,cal}$
1	1.20	1.95	0.61	0.50	4.0	6.0	0.402	−0.078	−0.072
2	1.20	1.50	1.01	0.50	4.0	6.0	0.410	−0.146	−0.141
3	1.20	1.50	1.63	0.50	4.0	6.0	0.403	−0.272	−0.265
4	1.20	1.50	1.06	0.50	4.0	6.0	0.606	−0.160	−0.157
5	4.01	1.97	0.20	0.50	4.0	4.0	0.175	0.305	0.241

using this model. Table 3 lists the cell operating parameters for the base case. Nafion 112 membrane is chosen unless it is pointed out otherwise in the text. In the simulations, one parameter is varied and the other parameters are kept constant.

Fig. 3(a) and (b) shows the cell potential as a function of current density for various relative humidities of inlet gases in the coflow and counterflow modes, respectively. Cell performance increases as the relative humidity of inlet reactant gases increases from 0 to 75%, due to the higher water content of membrane at higher relative humidity of inlet gases and lower membrane resistance. At average current density $I_{av} = 1.0$ A/cm^2, the cell potential varies from 0.709 V ($\alpha_a = \alpha_c = 0.25$) to 0.723 V (for $\alpha_a = \alpha_c = 0.75$) in the coflow mode, and the cell potential varies from 0.698 V (dry gas, for $\alpha_a = \alpha_c = 0.0$) to 0.723 V (for $\alpha_a = \alpha_c = 0.75$) in the counterflow mode. The model predicts that the cell cannot be operated with dry gases in the coflow mode. While the relative humidity of inlet reactant gases is higher than 75%, the performances of fuel cell are almost constant both in the coflow and counterflow modes. The reason why cell performances, at high humidity of inlet gases, are rather similar is that the decrease of membrane resistance is compensated by increase of cathode overpotential due to the liquid water. To reduce heat removal and liquid water in the cathode, relative humidity of inlet reactant gases should not be higher than 100%. It can be found that counterflow mode cannot show any advantageous while the reactant gases are high humidified or saturated.

Fig. 4 shows the water content of membrane in the counterflow mode. Current density is kept constant at 1.0 A/cm^2 and the fuel cell is operated with dry gases. The simulation results show that water content gradient across the membrane is high in the inlet region of hydrogen and that the water content of membrane is very low in the outlet region of hydrogen. It can be obtained that the water content gradient in *y*-direction is 2 orders higher than that in *x*-direction. Therefore, it is correct to neglect the diffusion of water in the membrane in *y*-direction.

Fig. 5 shows the distribution of current density along the gas channel for various relative humidities of inlet gases. Cell potential is keep constant at 0.7 V and average current density may be varied. In the inlet region of gases, the current density is very low with low humidity reactant gases in the coflow mode. It is due to the low water content of membrane in this region. In the outlet region of gases, the current densities decrease slightly along the flow channel due to the

Table 3
Operating parameter for the base case

Parameter	Value
I_{av}	1.0 A/cm^2
p_a	4×10^5 Pa
p_c	4×10^5 Pa
T	353 K
α_a	0.5
α_c	0.5
ξ_a	1.5
ξ_c	2.0

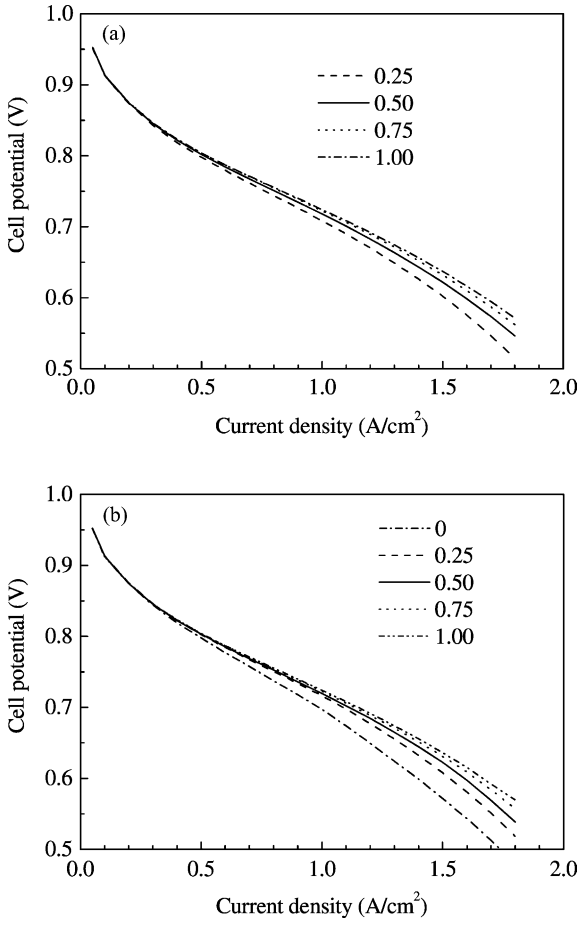

Fig. 3. The polarization curves for various relative humidities of inlet gases in the coflow (a) and counterflow (b) modes ($T = 353$ K, $p_a = p_c = 4 \times 10^5$ Pa, $\xi_a = 1.5$, $\xi_c = 2.0$, $\alpha_a = \alpha_c$).

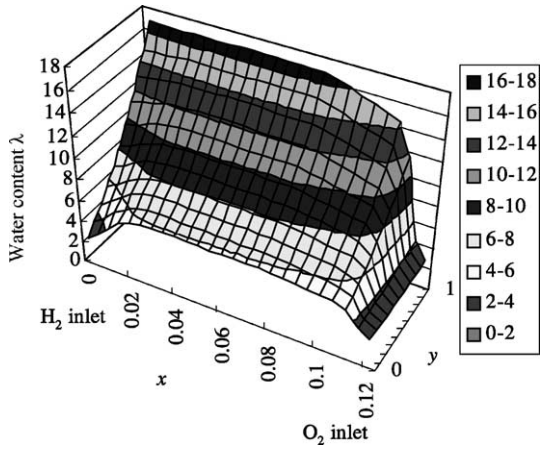

Fig. 4. Distribution of water content of membrane with dry gases in the counterflow mode ($T = 353\,\text{K}$, $I_{av} = 1.0\,\text{A/cm}^2$, $p_a = p_c = 4 \times 10^5\,\text{Pa}$, $\xi_a = 1.5$, $\xi_c = 2.0$).

existing of liquid water in the coflow mode. As discussed above, liquid water lowers the effective porosity for oxygen gas transport and increases the cathode overpotential. Compared to the coflow mode, counterflow mode improves

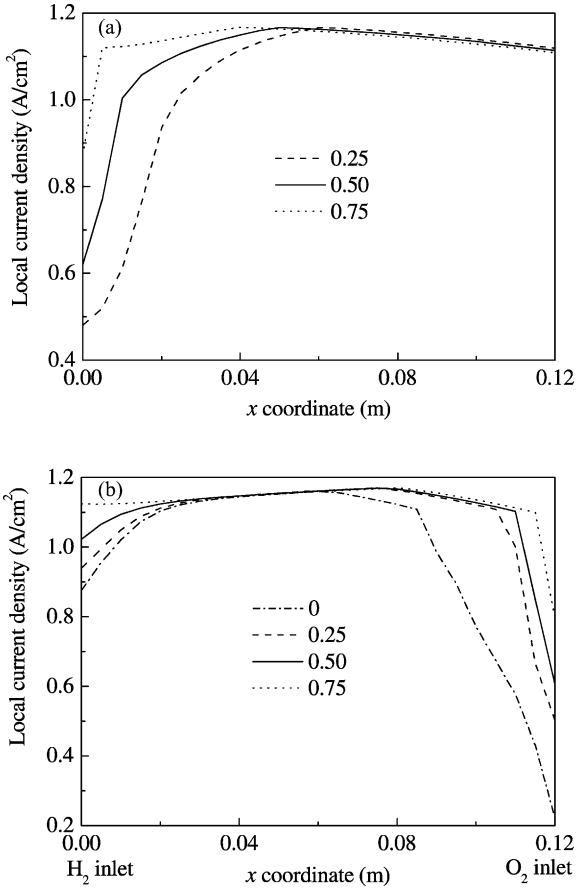

Fig. 5. Distribution of current density along the gas channel for various relative humidities of inlet gases in the coflow (a) and counterflow (b) modes ($T = 353\,\text{K}$, $E_{cell} = 0.7\,\text{V}$, $p_a = p_c = 4 \times 10^5\,\text{Pa}$, $\xi_a = 1.5$, $\xi_c = 2.0$, $\alpha_a = \alpha_c$).

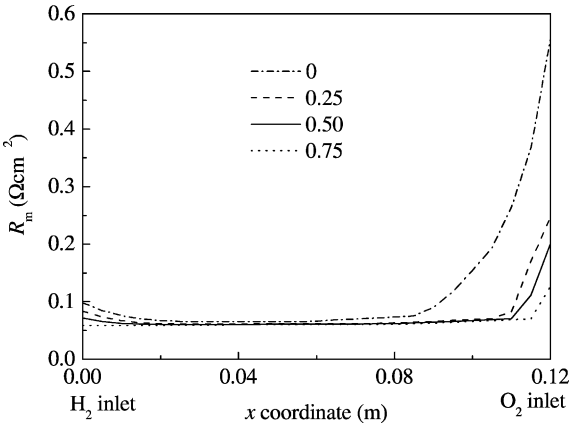

Fig. 6. Distribution of membrane resistance along the gas channel for various relative humidities of inlet gases in the counterflow mode ($T = 353\,\text{K}$, $I_{av} = 1.0\,\text{A/cm}^2$, $p_a = p_c = 4 \times 10^5\,\text{Pa}$, $\xi_a = 1.5$, $\xi_c = 2.0$, $\alpha_a = \alpha_c$).

the current density distribution with dry or low humidity gases.

Fig. 6 shows the distribution of membrane resistance along the gas channel for various relative humidity of gases. Current density is kept constant at $1.0\,\text{A/cm}^2$. The results show that the membrane resistances are high in the inlet and outlet regions of hydrogen due to low water content of membrane with dry or low humidity gases in counterflow mode.

Fig. 7 shows the distribution of fraction of water produced that transports through the anode along the gas channel for various relative humidities of gases. It can be found that the net flux of water across the membrane is not in the same direction over the entire area of the membrane in the fuel cell. The different directions of the flux of water across the membrane at different regions in the PEMFC results in an internal humidification of the reactant gases in counterflow operating with dry gases. On the dry hydrogen inlet region, where humidified oxygen exits the cell, the anode side of the membrane is dryer than the cathode side, thus

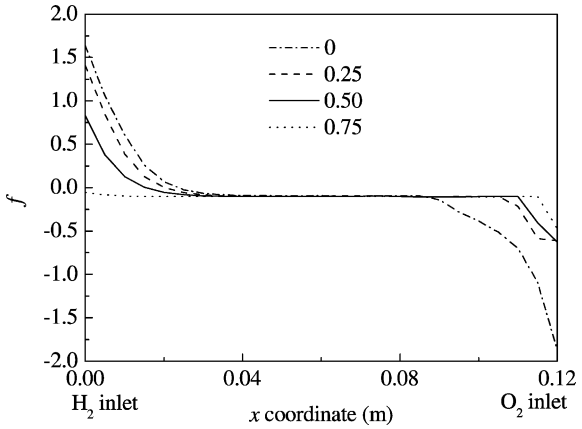

Fig. 7. Distribution of f along the gas channel for various relative humidities of inlet gases in the counterflow mode ($T = 353\,\text{K}$, $I_{av} = 1.0\,\text{A/cm}^2$, $p_a = p_c = 4 \times 10^5\,\text{Pa}$, $\xi_a = 1.5$, $\xi_c = 2.0$, $\alpha_a = \alpha_c$).

establishing a relatively steep water concentration gradient across the membrane (see Fig. 4). Water by electro-osmotic drag from the anode side to the cathode is lower than the back-diffusion water. It results in a net water flux from cathode to anode and the hydrogen is internally humidified. In the outlet region of hydrogen, where the dry oxygen enters and humidified hydrogen leaves the cell, water produced by electrochemical reaction is not enough to humidified dry oxygen, the cathode side of the membrane is dryer than the anode side, water is likely to be transported through the membrane from the anode side to the cathode side by electro-osmotic drag and diffusion [9]. The dry reactant gases can be internally well humidified and maintain high performance when PEMFC is operated in the counterflow mode without external humidification. The more the anode is humidified, the more water will migrate from anode to cathode in both coflow and counterflow modes.

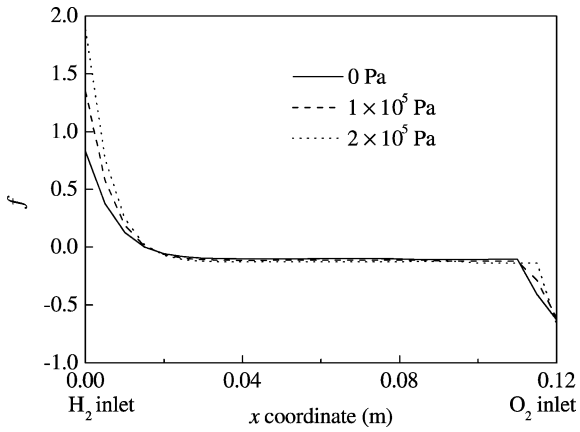

Fig. 9. Distribution of f for various pressure differentials along the gas channel in the counterflow mode ($T = 353\,\mathrm{K}$, $I_{av} = 1.0\,\mathrm{A/cm^2}$, $p_a = 4 \times 10^5\,\mathrm{Pa}$, $\xi_a = 1.5$, $\xi_c = 2.0$, $\alpha_a = \alpha_c = 0.5$).

3.3. Effect of pressure differential

Net water transport in the membrane arises from three mechanisms: electro-osmotic drag, diffusion and convection. At low current density, water content gradient in the membrane is not steep and water content of membrane on the anode side is high enough to keep the membrane proton conductivity well. At high current density, water transport by electro-osmotic drag is high and back diffusion water by the concentration gradient of water is insufficient to replenish the water loss. Membrane on the anode side will be dehydrated and membrane resistance increases in this case. Pressure differential can be used to force water transport from cathode to anode.

Figs. 8 and 9 show the distribution of membrane resistance and fraction of water produced that transports through the anode in the counterflow mode. While the anode pressure is kept constant at 4×10^5 Pa, three cathode pressures, 4×10^5, 5×10^5 and 6×10^5 Pa, are evaluated. The results show that higher pressure differential results in lower membrane resistance over the whole region along the flow channel and higher cell performance. A higher pressure differential results in higher value of f, that is to say, more water discharge from anode. Therefore, a higher cathode pressure can be used to reduce the anode dehydration problem and improve the fuel cell performance. However, it is possible for the thin Nafion membrane to be damaged if high pressure differential used is too high. In addition, high pressure differential may result in seal problem in fuel cell, especially in fuel cell stacks.

3.4. Effect of cell temperature

Fig. 10 shows the polarization curves for three different cell temperatures in the coflow mode. The results show that fuel cell performances increase with increasing temperature in range of 313–353 K. Water content in the anode side of membrane increases and membrane resistance decreases with increasing back diffusion coefficient of water in membrane. In addition, liquid water limits the transport of

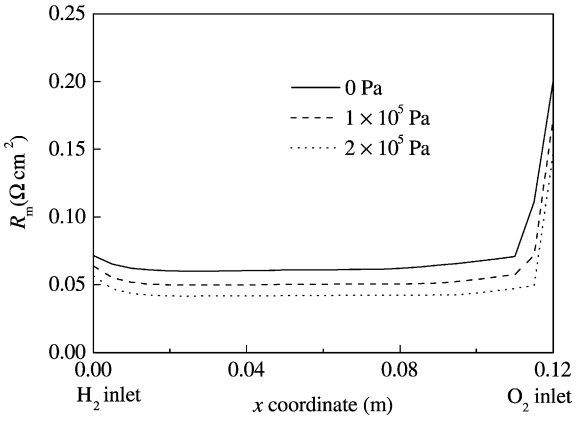

Fig. 8. Distribution of membrane resistance for various pressure differentials along the gas channel in the counterflow mode ($T = 353\,\mathrm{K}$, $I_{av} = 1.0\,\mathrm{A/cm^2}$, $p_a = 4 \times 10^5\,\mathrm{Pa}$, $\xi_a = 1.5$, $\xi_c = 2.0$, $\alpha_a = \alpha_c = 0.5$).

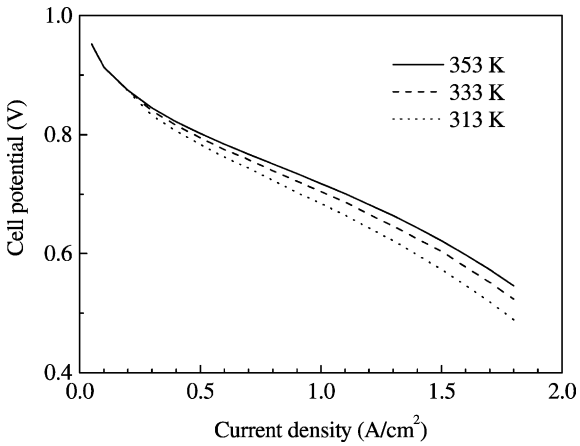

Fig. 10. The polarization curves for three different cell temperatures in the coflow mode ($p_a = p_c = 4 \times 10^5\,\mathrm{Pa}$, $\xi_a = 1.5$, $\xi_c = 2.0$, $\alpha_a = \alpha_c = 0.5$).

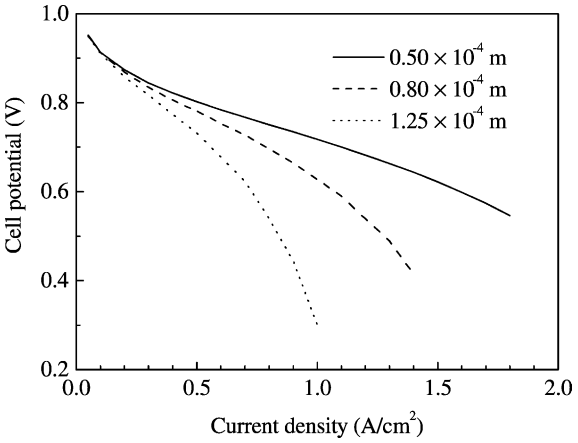

Fig. 11. The polarization curves for three thicknesses of membrane in the coflow mode ($T = 353$ K, $p_a = p_c = 4 \times 10^5$ Pa, $\xi_a = 1.5$, $\xi_c = 2.0$, $\alpha_a = \alpha_c = 0.5$).

reactant gases and covers part active site of electrode, when cell temperature increases, part of liquid water evaporates and cell performance increases. However, cell temperature should not be higher than 373 K because reactant gases are diluted by water vapor and lifetime of Nafion membrane decreases at high temperature.

3.5. Effect of membrane thickness

Fig. 11 shows the polarization curves for three thicknesses of membrane in the coflow modes. Cell performance increases with decreasing the thickness of membrane in the both modes, due to the higher water content of membrane and shorter distance of proton across the membrane. At average current density $I_{av} = 1.0$ A/cm^2, the cell potential varies from 0.718 V (for $\delta_m = 0.5 \times 10^{-4}$ m) to 0.301 V (for $\delta_m = 1.25 \times 10^{-4}$ m). Fig. 12 shows the water content profiles of membrane at $x = 0.06$ m in the coflow mode. Current density is kept constant at 1.0 A/cm^2. The simulation results show that the water content of membrane increases with decreasing the thickness of membrane, and water content gradient across the membrane is high for thick membrane. It seems that the thinner the membrane to be chosen as electrolyte, the better the cell performance. However, the difficulty of preparing membrane electrode assemble using thin membrane should be considered.

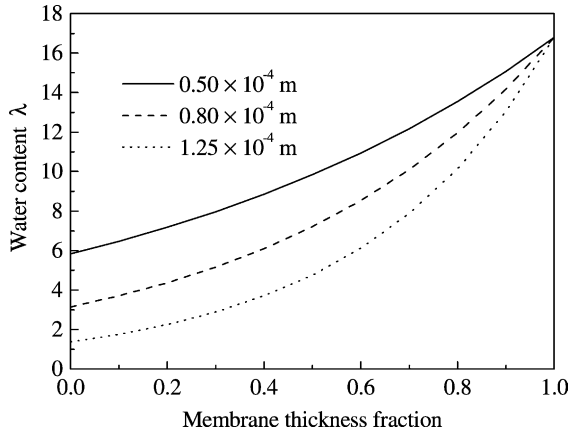

Fig. 12. The water content profiles for three thicknesses of membrane at $x = 0.06$ m in the coflow mode ($T = 353$ K, $I_{av} = 1.0$ A/cm^2, $p_a = p_c = 4 \times 10^5$ Pa, $\xi_a = 1.5$, $\xi_c = 2.0$, $\alpha_a = \alpha_c = 0.5$).

4. Conclusions

A two-dimensional model for a proton exchange membrane fuel cell was developed in which water transport in the membrane by electro-osmotic drag, back diffusion and pressure differential are included. Effect of liquid water on the effective porosity for gas transport in the cathode and cathode overpotential were considered. The model is used to investigate the effect of flow mode, operation conditions and membrane thickness on the water transport, water content of membrane and performance of fuel cell.

The simulations show that the water content of membrane and current density is very low in the inlet region of gases with low humidity gases in coflow mode. The dry reactant gases can be well internally humidified and maintain high performance when PEMFC is operated in counterflow mode without external humidification. Compared to the coflow mode, counterflow mode improves the current density distribution with dry and low humidity gases. Counterflow mode does not show any advantageous while the reactant gases are high humidified or saturated.

The performance of cell can be enhanced by increasing the temperature. Pressure differential can also be used to improve the cell performance. The results show that a higher cathode pressure can be used to reduce the anode dehydration problem. It is predicted in the model that the water content of membrane and cell performance increases with decrease in the thickness of the membrane. These studies will be useful for the design and operation of practical PEMFC stacks.

Calculated polarization curve compares very well with experimental results and calculated values for f_{av} are agreed with the experimental results.

Acknowledgements

This work was supported by Key Item of Knowledge Innovation Engineering of Chinese Academy of Sciences (KGCX1-SW-06) and by Postdoctoral Science Foundation of China.

References

[1] D. Rastler, J. Power Sources 86 (2000) 34–39.
[2] W. Smith, J. Power Sources 86 (2000) 74–83.
[3] P. Costamagna, S. Srinivasan, J. Power Sources 102 (2001) 242–252.

[4] C.K. Dyer, J. Power Sources 106 (2002) 31–34.
[5] K. Kordesch, G. Simader, Fuel Cells and Their Applications, VCH, Weinheim, Germany, 1996, 384 pp.
[6] T.E. Springer, M.S. Wilson, S. Gottesfeld, J. Electrochem. Soc. 140 (1993) 3513–3526.
[7] M. Watanabe, Y. Satoh, C. Shimura, J. Electrochem. Soc. 140 (1993) 3190–3193.
[8] C.S. Kong, D.Y. Kim, H.K. Lee, Y.G. Shul, T.H. Lee, J. Power sources 108 (2002) 185–191.
[9] F.N. Buchi, S. Srinivasan, J. Electrochem. Soc. 144 (1997) 2767–2772.
[10] Z. Qi, A. Kaufman, J. Power Sources 109 (2002) 469–476.
[11] D.R. Sena, E.A. Ticianelli, V.A. Paganin, E.R. Gonzalez, J. Electroanal. Chem. 477 (1999) 164–170.
[12] K.H. Choi, D.H. Peck, C.S. Kim, D.R. Shin, T.H. Lee, J. Power Sources 86 (2000) 197–201.
[13] T.E. Springer, T.A. Zawodzinski, S. Gottesfeld, J. Electrochem. Soc. 138 (1991) 2334–2342.
[14] D.M. Bernardi, M.W. Verbrugge, J. Electrochem. Soc. 139 (1992) 2477–2491.
[15] T.F. Fuller, J. Newman, J. Electrochem. Soc. 140 (1993) 1218–1225.
[16] T.V. Nguyen, R.E. White, J. Electrochem. Soc. 140 (1993) 2178–2186.
[17] V. Gurau, H. Liu, S. Kakac, AIChE J. 44 (1998) 2410–2422.
[18] I.M. Hsing, P. Futerko, Chem. Eng. Sci. 55 (2000) 4209–4218.
[19] K. Dannenberg, P. Ekdunge, G. Lindbergh, J. Appl. Electrochem. 30 (2000) 1377–1387.
[20] J.S. Yi, T.V. Nguyen, J. Electrochem. Soc. 146 (1999) 38–45.
[21] Z.H. Wang, C.Y. Wang, K.S. Chen, J. Power Sources 94 (2001) 40–50.
[22] D. Natarajan, T.V. Nguyen, J. Electrochem. Soc. 148 (2001) A1324–A1335.
[23] G.J.M. Janssen, J. Electrochem. Soc. 148 (2001) A1313–A1323.
[24] J.S. Yi, T.V. Nguyen, J. Electrochem. Soc. 145 (1998) 1149–1159.
[25] D.M. Bernardi, M.W. Verbrugge, AIChE J. 37 (1991) 1151–1163.
[26] R.B. Bird, W.E. Stewart, E.N. Lightfoot, Transport Phenomena, Wiley, New York, 1960.
[27] D.M. Bernardi, J. Electrochem. Soc. 137 (1990) 3344–3350.